Traveling-Wave Metal/Insulator/Metal Diodes for Improved Infrared Bandwidth and Efficiency of Antenna-Coupled Rectifiers

Sachit Grover, *Student Member, IEEE*, Olga Dmitriyeva, *Student Member, IEEE*, Michael J. Estes, *Member, IEEE*, and Garret Moddel, *Senior Member, IEEE*

***Abstract*—We evaluate a technique to improve the performance of antenna-coupled diode rectifiers working in the IR. Efficient operation of conventional, lumped-element rectifiers is limited to the low terahertz. By using femtosecond-fast MIM diodes in a traveling-wave (TW) configuration, we obtain a distributed rectifier with improved bandwidth. This design gives higher detection efficiency due to a good match between the antenna impedance and the geometry-controlled impedance of the TW structure. We have developed a method for calculating the responsivity of the antenna-coupled TW detector. Three TW devices, made from different materials, are simulated to obtain their impedance and responsivity at 1.5, 3, 5, and 10 μm wavelengths. The characteristic impedance of a 100-nm-wide TW is in the range of 50 Ω and has a small variation with frequency. A peak responsivity of 0.086 A/W is obtained for the Nb-Nb_2O_5-Nb TW diode at 3-μm wavelength. This corresponds to a quantum efficiency of 3.6% and is a significant improvement over the antenna-coupled lumped-element diode rectifiers. For IR imaging, this results in a normalized detectivity of 4×10^6 Jones at 3 μm. We have identified several ways for improving the detectivity of the TW detector. Possible methods include decreasing the diode resistance, reducing the noise, and increasing the effective antenna area.**

***Index Terms*—MIM tunnel diode, rectenna, surface plasmon, traveling wave (TW).**

I. Introduction

INFRARED detectors that are made from narrow-bandgap semiconductors require cooling to suppress the thermally generated dark current [1]. Such detectors operating at room temperature have a low SNR and hence a poor detectivity [2]. Proposed room temperature detection techniques include the antenna-coupled bolometer and the antenna-coupled rectifier. Though bolometric detectors [3] have been successfully used in IR cameras [4], their slow response limits the modulation bandwidth. On the other hand, antenna-coupled diode rectifiers that use a Schottky diode [5]–[7], or an MIM diode [8], are inherently fast. As explained in Section II, these are also referred to as the antenna-coupled lumped-element detectors. The MIM diode has a tunneling time for electrons on the order of 10^{-15} s [9], [10] and can be used for both detection and mixing of IR signals [11], [12]. Lumped-element detectors based on MIM diodes have been researched for more than three decades [13]–[18]. Despite the advantage of the small tunneling time for electrons, these detectors have had inadequate performance in the IR [19], [20]. We investigate a modified approach, the MIM-based antenna-coupled traveling-wave (TW) detector [21], [22], that overcomes the limitations faced by the lumped-element detectors.

In Section II, we examine the cause for the limited performance of the lumped-element detector and introduce the concept of the TW detector. In Section III, we describe the basic concepts and tools that are required to model the performance of the TW detector. Performance calculation for the TW detector and comparison with the lumped-element detector is given in Section IV. In Section V, we compare the TW detector with other IR detector technologies. We also list its advantages and examine the techniques for future improvement.

II. Theory of Operation

Lumped-element and TW detectors convert the incident electromagnetic (EM) wave to an electrical signal using a microantenna. The antenna feeds into a diode, which rectifies the electrical signal. The difference between the lumped-element and the TW techniques is twofold. First, they differ in the manner in which the signal is transferred from the antenna to the diode. Second, as the names suggest, the TW rectifies a wave, while the lumped element has the same signal appearing across the whole diode. We now look at each of these detectors in more detail.

In Fig. 1(a), we show the lumped-element detector, which consists of an antenna connected to a small-area diode. We model the antenna as a Thévenin equivalent and the diode as the parallel combination of a capacitor and a voltage-dependent resistor. The resulting small-signal circuit is shown in Fig. 1(b). Two conclusions can be drawn from this circuit regarding the operation of the detector. First, the bandwidth of the detector is limited by the capacitance of the diode (C_D) and the resistance of the antenna (R_A), as given by

$$\omega_C = (R_A C_D)^{-1}. \quad (1)$$

Manuscript received December 28, 2009; accepted April 29, 2010. Date of publication June 1, 2010; date of current version November 10, 2010. The review of this paper was arranged by Associate Editor A. A. Balandin.

S. Grover, O. Dmitriyeva, and G. Moddel are with the Department of Electrical, Computer and Energy Engineering, University of Colorado, Boulder, CO 80309 USA (e-mail: sachit.grover@colorado.edu; m2olga@gmail.com; moddel@colorado.edu).

M. J. Estes is with Zolo Technologies, Inc., Boulder, CO 80301 USA (e-mail: mestes@zolotech.com).

Color versions of one or more of the figures in this paper are available online at http://ieeexplore.ieee.org.

Digital Object Identifier 10.1109/TNANO.2010.2051334

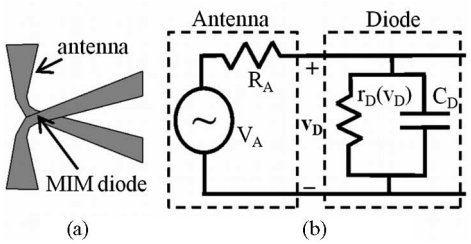

Fig. 1. (a) Antenna-coupled rectifier or the lumped-element detector. The IR signal received by the antenna is rectified in the diode formed at the junction of the antenna arms. The leads on the right side take the low-frequency signal out to a load. (b) Small-signal circuit representation of the detector. The antenna is represented by a Thévenin equivalent and the diode by the parallel combination of a voltage-dependent resistor and a capacitor. The signal bandwidth is limited by the $R_A C_D$ time constant. The impedance match between R_A and r_D determines the efficiency of power transfer from the antenna to the diode.

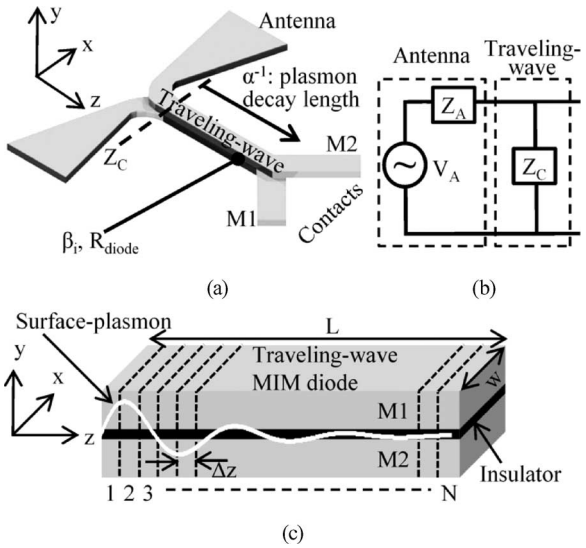

Fig. 2. (a) Isometric view of the antenna-coupled TW detector. The antenna arms converge into a parallel-plate waveguide with a thin (2 nm) insulator between the metals M1 and M2. On the other end, these metals form the leads to the contact pads (not shown) or the load. Parameters required for calculating the performance of the traveling wave include the characteristic impedance of the waveguide (Z_C); the plasmon decay length (α^{-1}); and the tunnel diode resistance ($R_{\rm diode}$) and responsivity (β_i). (b) Small-signal circuit representation of the detector. Impedance of the TW diode can be readily matched to the antenna ($Z_A = Z_C^*$). (c) 3-D view of the TW MIM diode. The structure has a length L and a width w. To calculate the responsivity, we divide the entire length of the TW into N equal sections of width Δz.

Second, for maximum power transfer from the antenna to the diode, the resistance of the diode should be equal to the antenna resistance. To ensure a high cutoff frequency, the C_D needs to be small, which implies a small area for the diode [19]. On the other hand, nominal antenna impedances are on the order of 100 Ω and impedance matching requires a diode resistance of that magnitude. As the diode capacitance is directly proportional and its resistance is inversely proportional to the area, these contradictory requirements are difficult to achieve. One possibility, for increasing the bandwidth, is to use a small-area, low-resistance MIM diode like the Ni-NiO-Ni [11]. However, this improvement is insufficient for operating at sub-10-μm wavelengths.

For efficient operation of an antenna-coupled rectifier in the IR, we proposed the TW detector in 2002 [21]. A 3-D view of this device is shown in Fig. 2(a). It consists of an antenna connected to the two metals M1 and M2, with a thin insulator between them. The MIM sandwich forms an extended MIM tunnel diode, which has the characteristics of a plasmonic waveguide [23]. The radiation received by the antenna excites a surface plasmon in the TW diode, which propagates in the z-direction. The plasmon develops a voltage between the two metal electrodes causing tunneling of electrons in the y-direction. The resulting current is rectified due to an asymmetry in the $I(V)$ characteristics about the bias point, as characterized by the diode responsivity discussed in Section III-A. Due to losses, the high frequency components of the rectified signal do not travel over a large distance. Thus the output at the contacts is a net dc current.

The technique of rectifying a surface-plasmon wave extends the bandwidth and provides a higher efficiency as compared to the lumped-element detector. In the TW detector, the antenna can be matched to the characteristic impedance of the waveguide, as shown in the equivalent circuit in Fig. 2(b). This leads to an improved power transfer from the antenna to the diode. Also, the distributed rectifier in the TW does not have an *RC* bandwidth limitation. In the next section, we explain the techniques required to model the performance of the TW detector.

A variation of the TW has been implemented [24] by coupling the antenna-coupled TW to a silicon waveguide.

III. Performance Modeling

The efficiency (η) of the lumped-element detector is determined by the combination of several factors [8] as given by

$$\eta = \eta_a \eta_s \eta_c \eta_j \tag{2}$$

where η_a is the efficiency of coupling the incident EM radiation to the antenna; η_s is the efficiency of propagating the collected energy to the junction of the antenna and the diode; η_c is the efficiency of coupling the antenna to the diode; and η_j is the efficiency of rectifying the power received in the diode.

A common measure of the efficiency of a detector is its responsivity, which gives the dc current or voltage produced per watt of incident radiation. For this, we set $\eta_j = \beta_i$ in (2), where β_i is the current responsivity of the tunnel diode and is discussed in Section III-A. The coupling efficiency between the antenna and the diode (η_c) can be calculated from the small signal circuit model, as shown in Fig. 1(b). As the antenna efficiency $\eta_a \eta_s$ remains the same for both the TW and the lumped-element configurations, we normalize the detector responsivity with respect to this factor. Then the responsivity of the lumped-element detector is given by

$$\Re_{LE} = \eta_c \beta_i. \tag{3}$$

A similar estimate can be made for the performance of the TW detector. To model the responsivity of the distributed rectifier, we divide the MIM waveguide into N parts of width Δz, as shown in Fig. 2(c). The antenna excites a surface-plasmon wave in the MIM waveguide. Assuming that a power of 1 W is incident on the waveguide cross section (x–y), this wave develops a certain

voltage distribution ($V_{1W}(z)$) between the two metal plates. The 1 W of power is chosen for normalization. In reality, the incident power would be several orders-of-magnitude smaller. Resistive losses in the metal cause the plasmon-wave amplitude to decay exponentially along the z-axis. The resulting voltage distribution is given by

$$V_{1W}(z) = V_0 e^{-\alpha z} \tag{4}$$

where α is the decay constant or the inverse of the decay length of the plasmon, and V_0 is the voltage at $z = 0$. Here, we have ignored the decay of the plasmon wave due to rectification. As calculated in Section IV, the rectified energy is a small fraction of the total. To simplify the derivation, we assume a constant voltage distribution along the x-axis. The net power rectified in the diode is given by the following sum:

$$P_{\text{rect}} = \sum_{1}^{N} \left(\frac{V_{1W}^2(z)}{2R_{D/A}(w\Delta z)} \right) \tag{5}$$

where $R_{D/A}$ is the resistance per unit area of the diode, and w is the width along the x-axis. The dc current that results from P_{rect} is given by

$$i_{\text{dc}} = \beta_i P_{\text{rect}}. \tag{6}$$

Combining (5) and (6) and applying the limit of $N \to \infty (\Delta z \to 0)$, we obtain

$$i_{\text{dc}} = \frac{\beta_i V_0^2 w}{2R_{D/A}} \left(\frac{1 - e^{-2\alpha L}}{2\alpha} \right) \tag{7}$$

where L is the length of the waveguide. Since the incident power was normalized to 1 W, the dc current in (7) also gives the responsivity. If we choose the length of the waveguide to be larger than the decay length of the surface plasmon $\alpha L > 1$, then we can approximate the responsivity as

$$\Re_{TW} = \frac{\beta_i V_0^2}{4R_{D/A}} \frac{w}{\alpha}. \tag{8}$$

Equation (8) provides an estimate for the efficiency of the TW detector and helps to identify the ways for improving the device. Techniques for improvement are discussed in Section V-A.

We now describe how to obtain the parameters required to compute the responsivity, using (8). In Section III-A, we discuss the properties of the tunnel diode (β_i and $R_{D/A}$). In Section III-B, we explain the method for calculating the V_0, α, and the characteristic impedance of the TW. Using these quantities, we estimate the performance of the TW detector in Section IV.

A. Diode Resistance and Responsivity

Only at a low (subterahertz) frequency can a tunnel diode be considered to be a classical rectifier [25]. When the quantum energy of the incident photons ($V_{\text{ph}} = \hbar\omega/e$) exceeds the scale of nonlinearity or the turn-ON voltage of the diode, a semiclassical analysis for the photon-assisted tunneling is required [26], [27]. In this case, the resistance and responsivity take the finite difference form, respectively, given by

$$R_{D/A} = \frac{1}{I'} \to \frac{2(\hbar\omega/e)}{J(V_{\text{bias}} + \hbar\omega/q) - J(V_{\text{bias}} - \hbar\omega/q)} \tag{9a}$$

$$\beta_i = \frac{1}{2}\frac{I''}{I'} \to \frac{q}{\hbar\omega} \times \left[\frac{J(V_{\text{bias}} + \hbar\omega/q) - 2J(V_{\text{bias}}) + J(V_{\text{bias}} - \hbar\omega/q)}{J(V_{\text{bias}} + \hbar\omega/q) - J(V_{\text{bias}} - \hbar\omega/q)} \right] \tag{9b}$$

where $J(V)$ is the dc current density, and V_{bias} is the applied dc voltage. In the limit of $\hbar\omega/e \to 0$, the finite difference forms give the same values as the classical results.

The semiclassical formulas in (9a) and (9b) give a lower resistance and higher responsivity as compared to their classical limits. From (8), we can see that this is an advantage as it helps to increase the responsivity of the TW.

B. Traveling-Wave Characteristics

To find the parameters for the TW, we first find the TM modes of an MIM waveguide. To simplify the analysis, we assume that the waveguide is infinite in the x-direction, ensuring that only TM modes exist. These modes can have an even- or an odd-symmetric field distribution [28]. The incoming radiation induces an odd-symmetric current variation on the antenna arms, which matches with the odd TM mode of the MIM waveguide. By designing the TW diode to have characteristic impedance equal to the antenna impedance, the impedance matching and the mode matching allow efficient coupling between the antenna and the rectifier [21].

We calculate the complex propagation constant ($\gamma = \alpha + jk$) of the infinite waveguide by using a matrix method [29] to obtain the dispersion relation for the TM mode. With this estimate for γ and fixing the width of the waveguide to 100 nm, we solve for the corresponding hybrid mode (TE + TM), using a commercial finite element solver [30]. This provides an accurate propagation constant (γ) from which we can calculate the plasmon wavelength and the distance over which it propagates. The solver also provides the field distribution in the 2-D cross section of the waveguide. In Fig. 3, we plot these results for a Ni-NiO-Ni (MIM) TW structure simulated at 100 THz. As seen in Fig. 3(a), the wave is confined mainly to the 2-nm-thick insulator region. From the field distribution, the characteristic impedance [31] of the TW structure is

$$Z_C = \frac{V}{I} = \frac{\int_{M1}^{M2} \vec{E}.dy}{\oint \vec{H}.d\vec{r}} = \frac{\int_{M1}^{M2} E_Y\, dy}{\int_{-\infty, y=0}^{\infty} H_X\, dx}. \tag{10}$$

Here, the voltage is given by the integral of the electric field, which is shown in Fig. 3(b). The current is calculated using Ampère's law by integrating the magnetic field in a semi-infinite loop around either of the conductors. As seen in Fig. 3(c), the magnetic field falls rapidly outside the waveguide. Thus at an infinite distance, it is negligible and the current can be approximated by an integral along the x-axis from $-\infty$ to $+\infty$. For the validity of the aforementioned formula, the metal needs to be

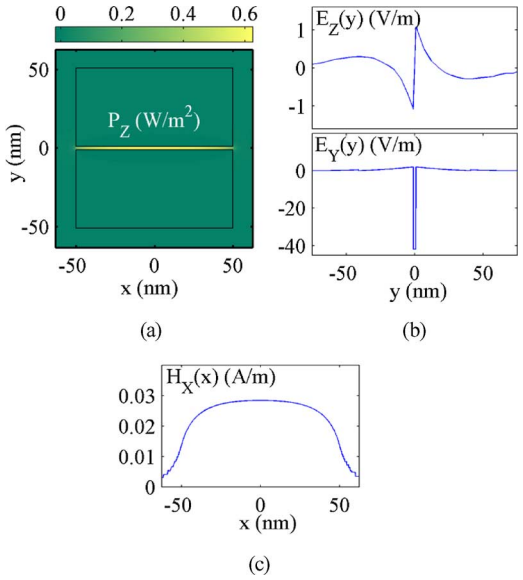

Fig. 3. Finite element analysis of a Ni-NiO-Ni TW diode for 100 THz. (a) Cross-sectional distribution of power flowing in the z-direction. The black rectangles mark the metal regions of the MIM diode. The power is confined mainly to the 2-nm-thick insulator. (b) The y- and z-directed electric fields as a function of the vertical position for $x = 0$. (c) The x-directed magnetic field as a function of the horizontal position for $y = 0$. The $E_Y\,(y)$ and the $H_X\,(x)$ are used to calculate the characteristic impedance of the traveling wave, which is 45 Ω for this analysis.

a perfect electric conductor or have its magnitude of dielectric constant much larger than the insulator $|\varepsilon_{\text{metal}}| \gg \varepsilon_{\text{insulator}}$. At IR wavelengths, the latter is the case for the materials that we have used.

Next, we calculate the V_0, which is proportional to the voltage given by the numerator of (10). Since V_0 corresponds to an incident power of 1 W, we apply a normalization factor given by the integration of the z-directed power density in the cross section of the TW. This leads to

$$V_0 = \frac{\int_{M1}^{M2} E_y\,dy}{\int_{area} P_Z\,dA}. \tag{11}$$

Using the aforementioned results, we calculate the performance of the TW in the next section.

IV. Performance Calculation

As explained in Section II, the TW diode facilitates a good impedance match between the antenna and the diode. Also, the distributed rectifier allows efficient operation at IR frequencies. Using the techniques described in Section III, we quantify these attributes by calculating the characteristic impedance and the responsivity of the TW. We choose to analyze these properties for three MIM material combinations that provide a small resistance ($R_{D/A}$) for the tunnel barrier. As given by (8), a small resistance is required to obtain a high responsivity for the TW detector. We compare the results for the Ni/NiO/Ni (0.2 eV) [24], the Nb/Nb_2O_5/Nb (0.1 eV) [32], and the Ta/Ta_2O_5/Ta (0.4 eV) tunnel diodes. The bracketed quantity denotes the barrier height of each diode. Symmetric tunnel barriers have been chosen to keep the analysis simple.

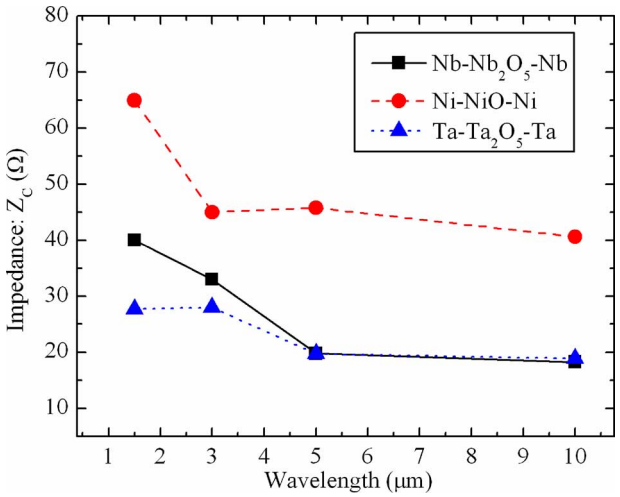

Fig. 4. Calculated characteristic impedance (Z_C) of the TW diode versus free-space wavelength. Three symmetric MIM structures have been analyzed. The values for Z_C are in the range of typical antenna impedances. Tuning of the impedance is possible by varying the width of the TW diode.

A. Characteristic Impedance and Responsivity

The characteristic impedance (Z_C) of the TW diode is plotted as a function of wavelength (1.5–10 μm) in Fig. 4. The Z_C is well within the range of typical antenna impedances. For a precise match with the antenna, we can fine tune the impedance of the TW diode by varying its width along the x-axis. The impedance match can be achieved over a large wavelength range, which is useful for broadband detection. The small variation in impedance with frequency is attributed to variation in the experimental values for the metal dielectric constants ($\varepsilon_{\text{metal}}$) [33], [34]. The impedances for the Nb and Ta devices are comparable as their $\varepsilon_{\text{metal}}$ are similar.

We calculate the responsivity of the TW diode at a dc bias of 0.1 V. This ensures an operating point at which the diode responsivity (β_i) is nonzero. We assume that a perfect impedance match can be made between the TW diode and the antenna ($\eta_c = 1$). The detector responsivity calculated from (8) is shown in Fig. 5. The responsivity of the TW detector is significantly improved and much less frequency dependent than the previous lumped-element detector. Details regarding this comparison are given in Section IV-B. The responsivity is higher for the low-barrier MIM diodes with the maximum for the Nb diode. The peak in the curves for Nb and Ni, and its absence in Ta, can be explained from the trends in resistance ($R_{D/A}$) and responsivity (β_i). These quantities vary with frequency as given in (9). Since the Ta-Ta_2O_5-Ta is a higher tunnel barrier than the Nb and Ni MIM diodes, it has a different variation of $R_{D/A}$ and β_i due to its larger turn-ON voltage.

B. Comparison With Lumped-Element Detector

We compare the responsivity of the TW detector with a lumped-element detector that has an antenna impedance of 100 Ω and a diode area of 100×100 nm^2. Both the detectors are made from the Nb-Nb_2O_5-Nb MIM diode. The resulting comparison is shown in Fig. 6. For the lumped-element device,

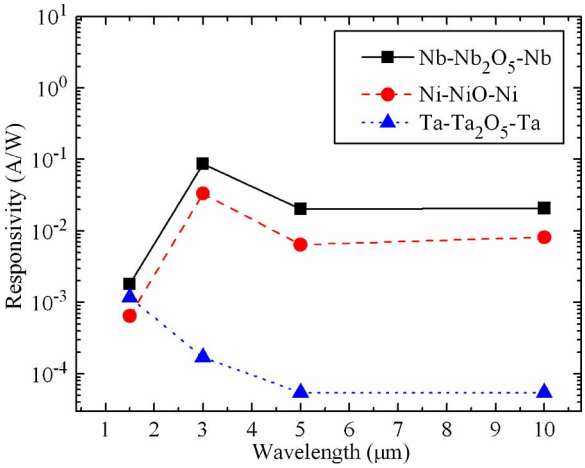

Fig. 5. Calculated responsivity of the TW diode versus free-space wavelength. The responsivity is higher for Ni and Nb since they have a lower barrier oxide than Ta. The peak in responsivity of the Nb device corresponds to a quantum efficiency of 3.6%.

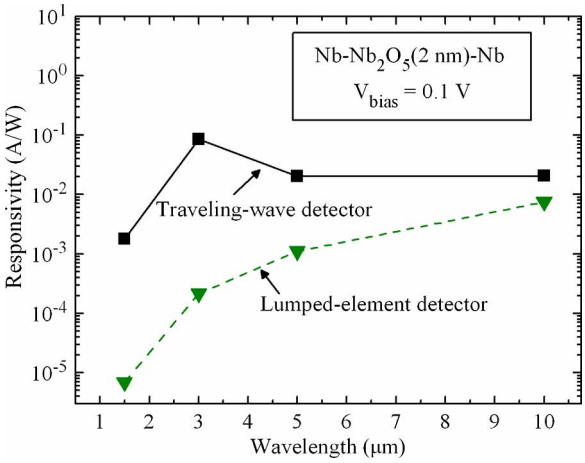

Fig. 6. Calculated responsivity comparison of the lumped-element and the TW detectors. The TW detector shows significantly better performance that does not degrade at smaller wavelengths. The responsivity of the lumped-element detector decreases as the diode admittance increases with decreasing wavelength.

the calculation is based on (3), in which we account for the impedance mismatch and the diode responsivity. The performance of the lumped-element detector degrades with increase in frequency. This is due to the decreasing admittance of the diode capacitor. A minor improvement in the lumped-element device can be achieved by choosing a smaller area for the diode.

V. Comparison With IR Detectors

In order to compare the TW detector with other detector technologies used for IR imaging, we have to calculate its normalized detectivity (D*) [1]. The D* is a measure of the noise performance of the detector and is defined as

$$\mathrm{D}^* = (A_d \Delta f)^{1/2} \frac{\Re_{TW}}{I_n} \tag{12}$$

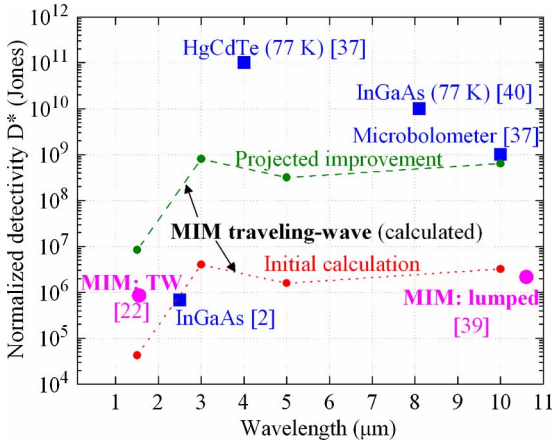

Fig. 7. Calculated detectivity comparison of the TW detector with semiconductor, thermal, and MIM lumped-element detectors. The initial calculation of the TW device response is based on the Nb-Nb_2O_5-Nb device. With improvements, the performance of the TW detector can be at par with thermal detectors.

where A_d is the detector area over which the radiation is received, Δf is the bandwidth of the readout circuitry, and I_n is the noise current in the diode.

We take the I_n to be a combination of Johnson and shot noise [35]. In Fig. 7, we compare the calculated D* of the TW detector with some of the existing technologies. The initial calculation corresponds to the Nb/Nb_2O_5/Nb TW detector responsivity, as shown in Fig. 6. The D* for the experimental TW detector [22] is close to the predicted performance. The curve for the projected improvement in performance is based on several factors explained in Section V-A. If implemented, the improved noise performance will place the TW detector at par with thermal detectors [1].

A significant advantage of the TW detector over the semiconductor-based ones is its ease of fabrication. With a small number of steps involving lithography and deposition of amorphous thin films, the detector can be easily made into a focal-plane-array on top of existing CMOS circuits. The spectral response of the traveling wave can be tuned with an appropriate design for the antenna [12]. Since the antenna detects the phase of the incoming signal [36], the traveling wave can be used in IR phased arrays. Unlike thermal detectors [Pg. 68, 37], the TW detector rectifies the incoming signal using tunneling and can support readout bandwidths in the terahertz. The large bandwidth is beneficial in communication applications where the detector can be used for sensing the envelope of amplitude-modulated signals [38].

A. Scope for Improvement

Three criteria for improving the performance of the TW detector can be identified from (12). Since the detector is not limited by background radiation noise, i.e., it is not a background limited infrared photodetector (BLIP) [Pg. 16, 37], we can increase the receiving area without affecting the noise performance. We can also increase the responsivity of the TW diode given in (8). This can be done by improving the design of the

TW structure and/or by using a diode with low resistance and high responsivity. These diode characteristics can be achieved by appropriately designing a multiinsulator diode [25]. Finally, reducing the current noise I_n can also improve D^*. This can be done by eliminating the shot noise, which is proportional to the dc current of the diode by operating at zero bias. For detector to work at zero bias, MIM diodes with asymmetric $I(V)$ characteristics close to the origin are required.

VI. Conclusion

For IR detection, the TW structure can improve the responsivity and bandwidth of antenna-coupled tunnel junctions. The innovation of this device is in having an MIM waveguide-cum-diode that rectifies the plasmon wave as it propagates. The distributed-rectifier improves the impedance match with the antenna and removes the *RC* limitation on bandwidth. We have derived a formula for calculating the responsivity of the TW diode that shows improving performance with increasing diode responsivity and reduced resistance. A multiinsulator diode can be designed to meet these requirements. From a calculation of the impedance and responsivity of the TW detector using experimental parameters for barrier heights and dielectric constants, we found that a good impedance match between the antenna and the TW can be realized. The responsivity of the TW detector is higher than that of the lumped-element detector, with scope for further improvement in it. Both the impedance and the responsivity allow the detection bandwidth to extend over several micrometer in the MWIR and the LWIR ranges. The spectral response will be determined by the design of the antenna.

With its projected performance capability on par with thermal detectors, the TW detector can be used in a range of applications including active IR imaging. The femtosecond-fast tunnel diode allows detection of signals with a modulation bandwidth that may extend into the terahertz. Finally, CMOS compatibility of the MIM technology means easy integration and low cost for these detectors.

Acknowledgment

The authors would like to thank Prof. E. F. Kuester for useful discussions on this topic.

References

[1] A. Rogalski, "Infrared detectors: Status and trends," *Progr. Quantum Electron.*, vol. 27, no. 2–3, pp. 59–210, 2003.

[2] P. V. Jayaweera, S. G. Matsik, A. G. Perera, H. C. Liu, M. Buchanan, and Z. R. Wasilewski, "Uncooled infrared detectors for 3-5 μm and beyond," *Appl. Phys. Lett.*, vol. 93, no. 2, pp. 021105-1–021105-3, 2008.

[3] P. L. Richards, "Bolometers for infrared and millimeter waves," *J. Appl. Phys.*, vol. 76, no. 1, pp. 1–24, Jul. 1997.

[4] W. A. Radford, R. Wyles, J. Wyles, J. B. Varesi, M. Ray, D. F. Murphy, A. Kennedy, A. Finch, E. A. Moody, F. Cheung, R. Coda, and S. T. Baur, "Microbolometer uncooled infrared camera with 20-mK NETD," in *Proc. Infrared Technol. Appl. XXIV*, San Diego, CA, 1998, vol. 3436, pp. 636–646.

[5] H. W. Hübers, G. W. Schwaab, and H. P. Röser, "Video detection and mixing performance of GaAs Schottky-barrier diodes at 30 THz and comparison with metal-insulator-metal diodes," *J. Appl. Phys.*, vol. 75, no. 8, pp. 4243–4248, 1994.

[6] H. Kazemi, K. Shinohara, G. Nagy, W. Ha, B. Lail, E. Grossman, G. Zummo, W. R. Folks, J. Alda, and G. Boreman, "First THz and IR characterization of nanometer-scaled antenna-coupled InGaAs/InP Schottky-diode detectors for room temperature infrared imaging," in *Proc. Infrared Technol. Appl. XXXIII*, 2007, vol. 6542, no. 1, pp. 65421J-1–65421J-4.

[7] E. R. Brown, "A system-level analysis of Schottky diodes for incoherent THz imaging arrays," *Solid-State Electron.*, vol. 48, pp. 2051–2053, Mar. 2004.

[8] B. M. Kale, "Electron tunneling devices in optics," *Opt. Eng.*, vol. 24, no. 2, pp. 267–274, 1985.

[9] T. E. Hartman, "Tunneling of a wave packet," *J. Appl. Phys.*, vol. 33, no. 12, pp. 3427–3433, Dec. 1962.

[10] M. Nagae, "Response time of metal-insulator-metal tunnel junctions," *Jpn. J. Appl. Phys.*, vol. 11, no. 11, pp. 1611–1621, Nov. 1972.

[11] M. Heiblum, S. Wang, J. Whinnery, and T. Gustafson, "Characteristics of integrated MOM junctions at dc and at optical frequencies," *IEEE J. Quantum Electron.*, vol. QE-14, no. 3, pp. 159–169, Mar. 1978.

[12] C. Fumeaux, W. Herrmann, F. K. Kneubühl, and H. Rothuizen, "Nanometer thin-film Ni-NiO-Ni diodes for detection and mixing of 30 THz radiation," *Infrared Phys. Technol.*, vol. 39, no. 3, pp. 123–183, 1998.

[13] J. W. Dees, "Detection and harmonic generation in the submillimeter wavelength region," *Microwave J.*, vol. 9, pp. 48–55, Sep. 1966.

[14] S. Faris, T. Gustafson, and J. Wiesner, "Detection of optical and infrared radiation with DC-biased electron-tunneling metal-barrier-metal diodes," *IEEE J. Quantum Electron.*, vol. QE-9, no. 7, pp. 737–745, Jul. 1973.

[15] A. B. Hoofring, V. J. Kapoor, and W. Krawczonek, "Submicron nickel-oxide-gold tunnel diode detectors for rectennas," *J. Appl. Phys.*, vol. 66, no. 1, pp. 430–437, 1989.

[16] G. D. Boreman, "Infrared microantennas," in *Proc. 10th Meeting Opt. Eng. Israel*, 1997, vol. 3110, no. 1, pp. 882–885.

[17] M. R. Abdel-Rahman, F. J. Gonzalez, G. Zummo, C. F. Middleton, and G. D. Boreman, "Antenna-coupled MOM diodes for dual-band detection in MMW and LWIR," in *Proc. Radar Sens. Technol. VIII Passive Millimeter-Wave Imag. Technol. VII*, 2004, vol. 5410, no. 1, pp. 238–243.

[18] I. Codreanu, F. J. Gonzalez, and G. D. Boreman, "Detection mechanisms in microstrip dipole antenna-coupled infrared detectors," *Infrared Phys. Technol.*, vol. 44, no. 3, pp. 155–163, 2003.

[19] A. Sanchez, C. F. Davis, Jr., K. C. Liu, and A. Javan, "The MOM tunneling diode: Theoretical estimate of its performance at microwave and infrared frequencies," *J. Appl. Phys.*, vol. 49, no. 10, pp. 5270–5277, 1978.

[20] S. Marchetti, P. Sandri, and R. Simili, "Theoretical and experimental responsivity of fir antenna coupled metal-insulator-metal detectors," *Int. J. Infrared Millimeter Waves*, vol. 18, no. 11, pp. 2161–2175, Nov. 1997.

[21] M. J. Estes and G. Moddel, "Surface plasmon devices," U.S. Patent 7 010 183, 2006.

[22] "Infrared photon field detectors," Univ. Colorado and Phiar Corp., Final Report, 2002 (National Reconnaissance Office, DII program, Contract No. NRO000-01-C-0221).

[23] R. Zia, M. D. Selker, P. B. Catrysse, and M. L. Brongersma, "Geometries and materials for subwavelength surface plasmon modes," *J. Opt. Soc. Amer. A*, vol. 21, no. 12, pp. 2442–2446, Dec. 2004.

[24] P. C. Hobbs, R. B. Laibowitz, F. R. Libsch, N. C. LaBianca, and P. P. Chiniwalla, "Efficient waveguide-integrated tunnel junction detectors at 1.6 μm," *Opt. Expr.*, vol. 15, no. 25, pp. 16376–16389, 2007.

[25] B. J. Elliason, "Metal-insulator-metal diodes for solar energy conversion," Ph.D. dissertation, Univ. Colorado at Boulder, Boulder, 2001.

[26] P. K. Tien and J. P. Gordon, "Multiphoton process observed in the interaction of microwave fields with the tunneling between superconductor films," *Phys. Rev.*, vol. 129, no. 2, pp. 647–651, Jan. 1963.

[27] J. R. Tucker and M. J. Feldman, "Quantum detection at millimeter wavelengths," *Rev. Mod. Phys.*, vol. 57, no. 4, pp. 1055–1113, Oct. 1985.

[28] H. Raether, *Surface Plasmons, vol. 111 of Springer-Verlag Tracts in Modern Physics*. New York: Springer-Verlag, 1988.

[29] T. J. Davis, "Surface plasmon modes in multi-layer thin-films," *Opt. Commun.*, vol. 282, no. 1, pp. 135–140, 2009.

[30] COMSOL AB. *FEMLAB Electromagnetics Module User's Guide*, FEMLAB 3.1, 2004.

[31] J. Huang, T. Feichtner, P. Biagioni, and B. Hecht, "Impedance matching and emission properties of nanoantennas in an optical nanocircuit," *Nano Lett.*, vol. 9, no. 5, pp. 1897–1902, May 2009.

[32] R. J. P. Bain and G. B. Donaldson, "Sputtered all-niobium Josephson tunnel junctions with barrier oxide protected by gold," *J. Phys. C: Solid State Phys.*, vol. 18, no. 12, pp. 2539–2548, 1985.

[33] E. D. Palik, *Handbook of Optical Constants of Solids*. Orlando, FL: Academic, 1985.

[34] E. D. Palik, *Handbook of Optical Constants of Solids II*. San Diego, CA: Academic, 1991.
[35] H. Spieler, *Semicondutor Detector Systems*. New York: Oxford University Press, 2005.
[36] C. T. Middlebrook, P. M. Krenz, B. A. Lail, and G. D. Boreman, "Infrared phased-array antenna," *Microw. Opt. Technol. Lett.*, vol. 50, no. 3, pp. 719–723, 2008.
[37] A. Rogalski, *Infrared Detectors*. New York: Gordon and Breach, 2000.
[38] S. Rockwell, D. Lim, B. A. Bosco, J. H. Baker, B. Eliasson, K. Forsyth, and M. Cromar, "Characterization and modeling of metal/double-insulator/metal diodes for millimeter wave wireless receiver applications," in *Proc. Radio Freq. Integr. Circuits (RFIC) Symp., IEEE*, 2007, pp. 171–174.
[39] B. Tiwari, J. A. Bean, G. Szakmány, G. H. Bernstein, P. Fay, and W. Porod, "Controlled etching and regrowth of tunnel oxide for antenna-coupled metal-oxide-metal diodes," *J. Vacuum Sci. Technol. B: Microelectron. Nanometer Struct.*, vol. 27, no. 5, pp. 2153–2160, 2009.
[40] S. Gunapala, S. Bandara, C. Hill, D. Ting, J. Liu, J, Mumolo, S. Keo, and E. Blazejewski, "Quantum well and quantum dot based detector arrays for infrared imaging," in *Mater. Res. Soc. Symp. Proc.*, 2008, vol. 1076.

Sachit Grover (S'03) received the Bachelor of Technology degree in electrical engineering from the Indian Institute of Technology, Delhi, India, in 2006. He is currently working toward the Ph.D. degree at the Department of Electrical, Computer and Energy Engineering, University of Colorado, Boulder.

He is currently engaged in research on the development and analysis of high-speed diodes for antenna-coupled rectifiers that operate at infrared and visible wavelengths.

Olga Dmitriyeva (S'10) received the M.S. degree in physics from Voronezh State University, Voronezh, Russia, in 1996. She is currently working toward the Ph.D. degree at the Department of Electrical, Computer and Energy Engineering, University of Colorado, Boulder.

She was a Process Engineer at Picolight, Inc., and Phiar Corporation. Prior to that, she was a Research Assistant at the National Renewable Energy Laboratory, Golden, CO.

Michael J. Estes (M'03) received the B.S. degree from Ohio State University, Columbus, in 1985, the M.S. degree from the Air Force Institute of Technology, Wright-Patterson AFB, OH, in 1990, and the Ph.D. degree from the University of Colorado, Boulder, in 1995, all in electrical engineering.

He is currently the Director of Engineering at Zolo Technologies, Boulder, CO. He has more than 20 years of experience, leading technology and product development in the optics, laser, and optoelectronics fields. He was a cofounder and Director of engineering at Phiar Corporation, where he was involved in the development of terahertz diodes and transistors based on metal-insulator tunneling devices, and Engineering Manager at Melles Griot Electro-Optics, where he was involved in the development of diode laser products. He is a retired Air Force Reserve Lieutenant Colonel and spent 15 years as an active duty Air Force officer. He is the author or coauthor of 15 technical publications. He holds seven U.S. patents and has seven patent applications pending.

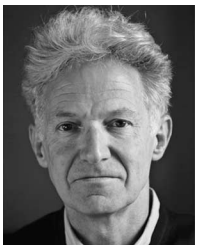

Garret Moddel (M'85–SM'93) received the BSEE degree from Stanford University, Palo Alto, CA, in 1976, and the M.S. and Ph.D. degrees in applied physics from Harvard University, Cambridge, MA, in 1978 and 1981, respectively.

After graduate school, he joined SERA Solar Corporation as a founding employee. In 1985, he joined the University of Colorado, Boulder, where he is currently a Professor at the Department of Electrical, Computer, and Energy Engineering. As a Professor, he has researched new thin-film optoelectronic materials and devices. His current research interests include quantum engineering of new thin-film metal devices for energy conversion and detection. He was the founding President and Chief Executive Officer of Phiar Corporation, which was started in 2001 for developing ultra-high-speed metal-insulator electronics.

Prof. Moddel is a Fellow of the Optical Society of America. He was named the first CU Inventor of the Year in the Physical Sciences in 2002.